Ultrafast nonlinearities of minibands in metallodielectric Bragg resonators

Petros Farah, Nicholas Gibbons, Fu Min Huang, and Jeremy J. Baumberg
NanoPhotonics Center, Cavendish Laboratory, University of Cambridge, Cambridge CB3 0HE, England, United Kingdom
(Received 22 June 2011; published 28 September 2011)

The nonlinear properties of metallodielectric DBRs are investigated via optical pump-probe techniques using a widely tunable, dual-colour, high-repetition rate, ultrafast setup. As a consequence of the Bragg-arranged multilayers, the electric field penetrates to different depths of the nanostructure at different excitation resonances, strongly enhancing the intrinsic nonlinear response of the metal in comparison with bulk films. The analyzed spectral response of these structures reveals how their nonlinear behavior is dominated by the pump-induced modification of the metal dielectric function. Fitting the simulated changes of the optical resonances using transfer-matrix methods matches experiment well, and shows the key effects of the spectral dependence of the spatial mode profiles.

DOI: 10.1103/PhysRevB.84.125442 PACS number(s): 42.70.Qs, 78.67.Pt, 42.65.−k, 72.15.Lh

I. INTRODUCTION

Distributed Bragg reflectors (DBRs) are ubiquitous for their high reflectivity, which is produced by the optical superposition setup in the multilayer structure. Their archetypal response consists of a high-reflectivity stopband surrounded by a series of highly transmissive minibands [see Fig. 1(a)]. Incorporating metals in such structures gives the opportunity to take advantage of the metallic nonlinear response, while maintaining low losses in the transmissive regime.[1] Such structures produce "transparent metals" with >50% transmittivity[2] easily obtained in high-quality DBRs.

Previous studies have shown that such multilayer structures enhance the nonlinear response by an order of magnitude compared to single metal films.[1,3,4] It has also been shown that such structures access second order $\chi^{(2)}$ nonlinearities of metals[5] enabling new devices with enhanced nonlinear properties. Furthermore, optical switches have been proposed that use the sharp change in the optical properties of these structures in the nonlinear regime.[6]

Here, we investigate the nonlinear optical response in such metallodielectic DBRs (MDDBRs) and extract the mechanisms behind the enhancement. It has previously been shown that the nonlinearity of MDDBRs spectrally follows their absorption.[7,8] Through measurements on samples with more stacked layers grown using a novel scalable technique,[2] which produces sharper Bragg resonances, we demonstrate that the absorption has an indirect role on the nonlinear response. By simulating the nonlinear response, we show that the main reason for the enhancement is the change of the combined structure's optical resonance resulting from the induced change of the metal optical properties. Furthermore, we demonstrate how the different spatial profiles of the resonant modes in the structures modify the energy deposited in the structure in unusual and novel ways.

II. SAMPLES AND SETUP

The nonlinear behavior of MDDBRs is investigated using a pump-probe technique. The samples were fabricated using release rollup assembly (RRA) as described by Gibbons *et al.*[2] The multilayers used here consist of four bilayers with 14 nm of gold and 212 nm of polydimethylsiloxane (PDMS) [see Fig. 1(d)] producing a stopband centered around $\lambda_m =$ 600 nm. Beyond the stopband, the transmission spectra of the sample exhibits a series of highly transmissive minibands [see Fig. 1(b)], discussed further in Sec. IV A. Below 500 nm, the absorption of the metal dominates, hence the sample exhibits low reflection and transmission in this region.

The samples were mounted in a goniometer setup enabling the angles of incidence to be independently selected without varying the pulse time of arrival at the sample. The pump and probe incident angles were fixed to 30° and 10°, respectively, in order to minimize stray pump reflection in the direction of the probe while staying close to normal incidence. Pump-probe measurements utilized 200-fs pulses with a maximum energy of 1 nJ at a repetition rate of 250 kHz. The pump pulses were modulated at 17 kHz using an acousto-optic modulator, sufficient to allow near-complete sample relaxation between pulses. A dual fs-synchronised Optical Parametric Amplifier (OPA) system allowed for widely tunable pulse wavelengths from 500 to 730 nm, independently for the pump and probe. The delay between the pump and probe pulses (Δt) was scanned while recording the normalized changes in reflectivity ($\frac{\Delta R}{R}$) and transmission ($\frac{\Delta T}{T}$) of the sample using standard balanced lock-in detection. The typical response (see Fig. 2) was found to contain three contributions as discussed below.

III. THE NONLINEAR RESPONSE OF METALS

The optical properties of coinage metals (Au, Ag, Cu) are dominated by the free valence electrons and are well described by the Drude model. Corrections to this model however need to be made for the interband transitions, which add to the absorption in these metals. In gold, a *d*-band-to-*p*-band transition occurs above 2.5 eV and is responsible for the yellowish color of the metal.[9] As discussed below, the interband transitions are the strongest contribution to the nonlinear response of gold since they excite electrons to the high-energy states from bonding states.

The nonlinear properties of noble metals, in particular, gold and silver, have been previously studied in thin films by broadband pump-probe[10,11] and $\mathcal{Z}$-scan (single wavelength) techniques.[12,13] Absorption is found to be the dominant cause of the nonlinear response of such metals.[12] The absorbed light

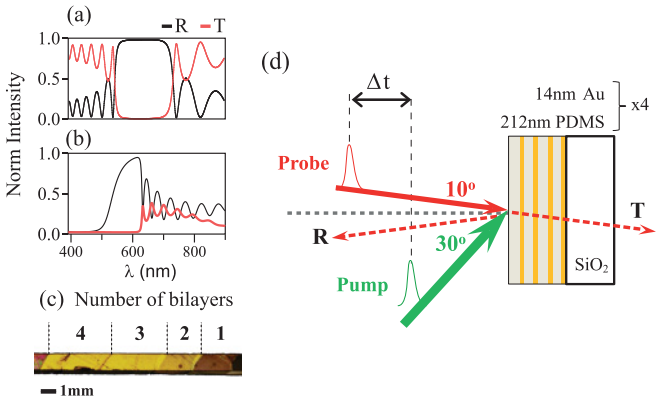

FIG. 1. (Color online) Characteristic reflection and transmission spectra of typical (a) DBR and (b) MDDBR with 10 bilayers demonstrating the high transmission peaks on the side of the stopband. (c) Image of the sample produced by release rollup assembly providing access to regions with different number of stacked bilayers. (d) Schematic of the pump-probe setup.

heats up the metal locally, modifying the optical properties through thermooptic coefficients. The Drude model, $\epsilon(\omega) = \epsilon_\infty(T) - \frac{\omega_p(T)^2}{\omega^2 + i\omega\gamma(T)}$, defines the thermooptic coefficients from the electron damping (γ), the plasma frequency (ω_p), and ϵ_∞, the sum of the interband contributions.[10] We note that the electron damping parameter includes contributions from the electron-electron, electron-phonon, and electron-surface phonon scattering. Here, we examine these dependencies in more detail using a two-temperature model.

A. The two-temperature model

A two-temperature (2T) model is generally employed to explain the temporal dynamics of the nonlinear response in metals. In the 2T model, the optical response of the valence electrons is initially decoupled from the lattice,[14–16] thus giving a three-step energy relaxation[17] (see Fig. 3). An incident pump pulse excites electrons from below the Fermi level producing a nonthermal distribution (N). Within a

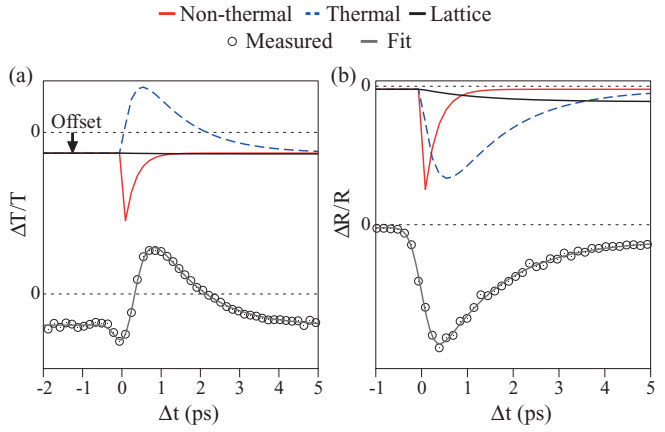

FIG. 2. (Color online) Bottom: examples of measured response (circles) along with fits (solid grey line) for (a) transmission and (b) reflectivity. Top: the four components used to produce the fits, as described by Eq. (1).

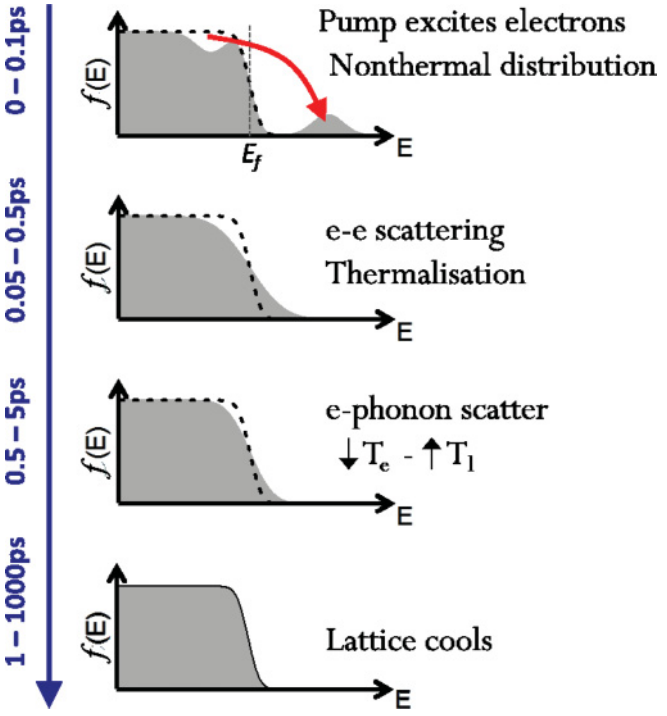

FIG. 3. (Color online) Schematic demonstrating how the electron distribution in a metal evolves in response to a pump pulse. The changes in the electron distribution modify the optical response of the metal, leading to the observed change in the dielectric constant.[17]

picosecond the electrons thermalize through electron-electron scattering leading to a Boltzmann or thermal distribution (T) at an elevated temperature. The hot electrons (thermal and nonthermal) slowly transfer energy to the lattice through electron-phonon coupling, hence heating up the lattice (L). On a much longer timescale, the hot lattice will thermalize with the surrounding medium.

The classical two-temperature model treats the relaxation of the thermalised electron distribution, but ignores the dynamics of the initial nonthermal electrons. As the electron thermalisation time is short compared with the pulse width, this can sometimes be justified. However, in the system studied here, the nonthermal and thermal responses are found to have opposing effects on the reflectivity or transmission of the sample, as seen in Fig. 2(a). Therefore incorporating the nonthermal electrons is vital in order to gain a more complete picture of the dynamics.

Approaches toward a more complete model incorporating the nonthermal response have recently been made by extending the 2T model rate equations[18] or by solving the Boltzmann equation for the electrons.[19] However, for the purposes of this study, a qualitative understanding of the dynamics along the lines presented by Sun *et al.*[19] is sufficient to understand the role of the resonant modes.

B. Fitting parameters

A simplified version of the 2T rate equations, shown in Eq. (1), is used here to fit the transient time evolution of the nonlinear response. The four components of the response result

from the nonthermal distribution of electrons (N), the thermal distribution of electrons (T), the lattice heating (L), and a long lived (constant) offset (C) discussed further below. These are dependent upon two decay rates, the electron-electron coupling rate (α) and the electron-phonon coupling rate (β). Equation (1) is convolved with a Gaussian to account for the instrumental time resolution at the sample, which was experimentally determined to be 0.3 ps.

$$\frac{\Delta R}{R} = \left(\frac{\Delta R}{R}\right)_C + \left[\left(\frac{\Delta R}{R}\right)_N e^{-t(\alpha+\beta)} + \left(\frac{\Delta R}{R}\right)_T (1-e^{-t\alpha})e^{-t\beta} + \left(\frac{\Delta R}{R}\right)_L (1-e^{-t\beta})\right]_{t>0} \quad (1)$$

The linear dependence of the electron-phonon coupling rate (β) with electron temperature[18] means that the rate evolves during the transient described by Eq. (1). Even though this evolution is not accounted for in this model, good qualitative results can still be obtained from this simplified model as has been shown by Sun *et al.*[19] The different contributions can be straightforwardly extracted from the data (see Fig. 2). The rise and fall times define the rates α and β and the amplitudes are extracted for each probe wavelength.

IV. MDDBR OPTICAL RESPONSE

A. Linear response

The linear response of the MDDBR is simulated using the transfer-matrix method.[20] A spectrally constant refractive index was assumed for the PDMS layers ($\tilde{n}_{\mathrm{PDMS}} = 1.41 + i0.001$) and the dielectric constant of gold was taken from the literature.[21] The good agreement of the simulated reflection and transmission spectra with experiment validates the model. Furthermore, the electric-field spatial profile across the spectrum can be extracted from the simulations. This provides a detailed understanding of where in the structure the pump energy is deposited. In addition, the dispersion relation in the direction perpendicular to the surface (see Fig. 4) is calculated from the complex transmisivity[22] providing insight into how the spectral features arise.

The main feature in the spectral response is the stopband around 600 nm, arising from the one-dimensional (1D) photonic crystal formed by the multilayer. Beyond the stopband, a series of reflection and transmission peaks are observed. The transmission peaks are equivalent to minibands formed by nearest-neighbor coupling between a series of identical microcavities.[23] In the MDDBR presented here, each PDMS layer is enclosed by gold mirrors, forming a series of microcavities, which couple leading to the splitting of their Fabry-Perot resonances, producing the observed transmission miniband. The dispersion relation in Fig. 4(b) shows that the discrete transmission peaks occur at the corresponding k states in the miniband.

The electric-field profile at key points in the spectrum shows strong variation of the deposited energy with depth [see Fig. 5(c)]. At the peak of the stopband (600 nm) the resonance leads to a minimum electric field inside the metal. At shorter wavelengths, a decaying electric-field profile penetrating the

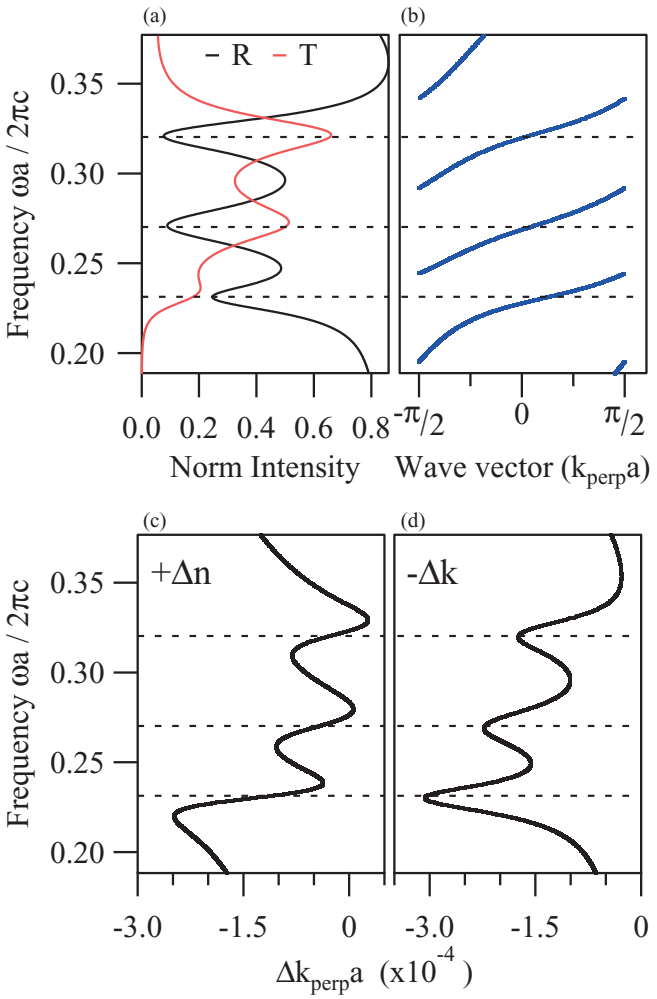

FIG. 4. (Color online) (a) Experimental reflection and transmission spectra showing the transmission minibands. (b) The corresponding folded dispersion relation demonstrates the resulting Bloch modes matching each resonance, where a (which is equal to 226 nm) is the thickness of the bilayer. The change of the dispersion caused by independently modifying the (c) real and (d) imaginary part of the refractive index.

sample is observed along with an increased total electric field in the gold layers, leading to larger absorption and reduced reflectivity [see Fig. 5(a)]. Within this wavelength range, interband transitions in the gold dominate causing the strong absorption observed. Toward longer wavelengths, different Bloch optical resonances in the structure lead to the localization of the electric field within different layers. For instance, the Bloch mode at 660 nm possesses an electric field envelope, which mostly injects energy into the first and last metal layers, whereas at 720 nm, most of the energy is injected into the second metal layer. However, at 600 nm, equal energies are deposited in each layer despite the decay of the overall envelope. Hence the pump deposits energy into the nm-scale thin Au layers in counter-intuitive ratios [see Fig. 5(b)].

B. Nonlinear response

In such MDDBRs, the nonlinear response on picosecond timescales is found to be predominantly due to the electronic

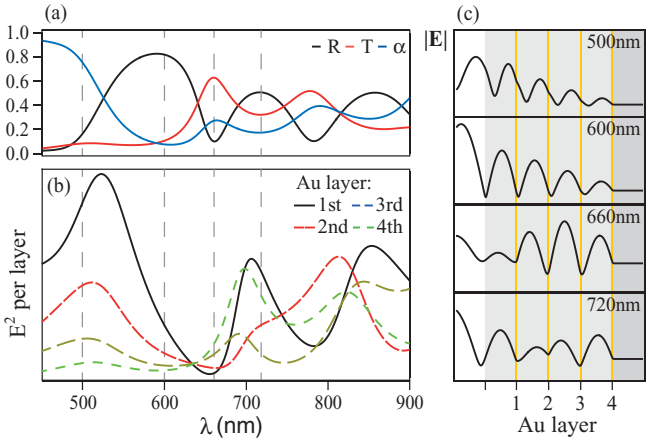

FIG. 5. (Color online) (a) Simulations of the linear reflection, transmission, and absorption spectra of the MDDBR at 30°. (b) Integrated optical field magnitude in each layer of Au. (c) Field distributions at selected wavelengths, indicated by dashed lines in (a). The gray regions indicate the PDMS and substrate (dark gray) and the yellow lines the gold layers.

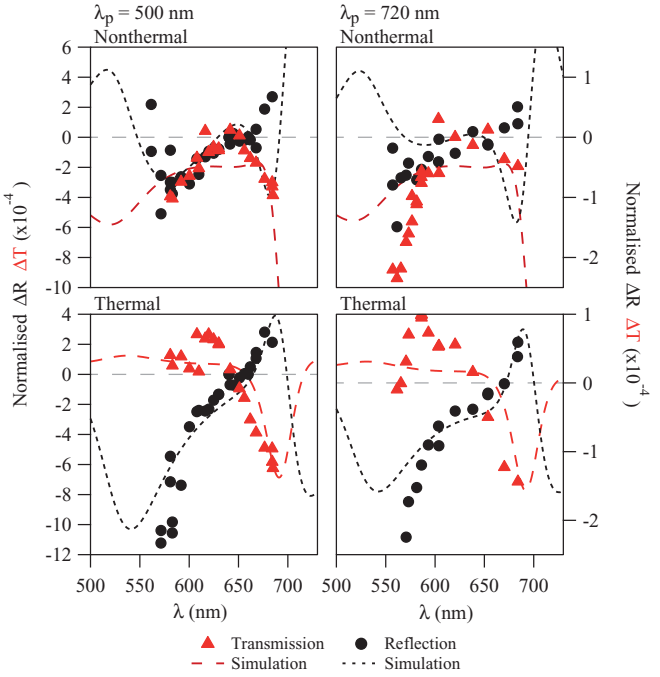

FIG. 6. (Color online) Spectral response of the reflectivity and transmisivity of the MDDBR to selective energy injection at specific pump wavelengths (λ_p). The nonthermal (fast) and thermal components are separately shown along with the simulated responses caused by perturbations of the gold complex refractive index given in Table I.

nonlinearities in the metal. Although the transparent polymer possesses a third-order nonlinear response, this is very small in comparison to the metal and is not taken into account here. Moreover, absorption of the polymer is negligible, hence no ultrafast transient thermal contributions from the polymer, such as thermal expansion, are present. As discussed in Sec. V C, thermal contributions are found at longer timescales, when the optically heated gold layers thermalize with the polymer layers.

To estimate the nonlinear response of the MDDBR, a perturbed dielectric function for gold is used for the transfer-matrix simulations. This perturbation is distributed between the gold layers in proportion to the integrated electric field amplitude per gold layer at the pump wavelength, shown in Fig. 5(b). The relative change in reflectance and transmittance between the linear and perturbed models is compared to the values of $\frac{\Delta R}{R}$ and $\frac{\Delta T}{T}$ obtained experimentally.

V. RESULTS AND DISCUSSION

A. Spectral response

The thermal and nonthermal responses of the system, when pumped at 500 and 720 nm with a pulse energy of 100 pJ, are shown in Fig. 6 alongside fits extracted from the model described in Sec. III B. The biggest predicted response is observed around 500 and 700 nm, which corresponds to either side of the stop band. In contrast, around the peak of the stopband at 600 nm, a spectrally flat response is observed. This implies that the main response arises from a shift in the spectral features rather than a change in their magnitude. This is particularly evident in the electronic thermal (T) response where a reduction in reflection around 550 nm is accompanied with an increase around 650 nm indicating a redshift of the stopband. The transmission miniband, which peaks around 700 nm, also experiences this redshift as demonstrated by the reduction in transmission below 700 nm. The nonthermal (N) components however generally show a reduction in both reflection and transmission indicating an increase in absorption.

In general, our model fits these features in the extracted experimental response very well. The main deviation from the modelled response occurs in the region below 600 nm where interband transitions are expected to have a strong effect on the nonlinear properties of the metal. We note that the nonthermal response is not modelled as accurately as the thermal response. Models of the interband absorption in the literature suggest that the nonthermal response possesses a stronger and more spectrally varying response.[19] Hence a larger deviation from our model is expected, since a spectrally constant response is used here.

The spectral shifts are a consequence of the modification of the optical resonances in the MDDBR, which can be caused by a change in the layer thickness and/or a change in the material optical constants. The PDMS layer absorption is observed to be negligible, so on the ps time scales we need consider only the gold layer response. While laser-induced thermal expansion of the gold layers can occur, it only arises on longer time scales than the transients here, and the resulting spectral effect expected from simulations does not match the observed response. Hence the response over ps time scales is attributed to the transient change of the gold dielectric function. As discussed in Sec. IV B, we account for this change in our transfer matrix model with a perturbation of the complex index of refraction of gold ($\Delta\tilde{n}_{\mathrm{Au}}$), distributed amongst the metal layers in proportion to the integrated local optical intensity per layer. The value for the total $\Delta\tilde{n}_{\mathrm{Au}}$ was chosen to give the best agreement with experiment (Table I).

TABLE I. Total change in the complex index of refraction (sum of all four gold layers) found to best fit the obtained spectral response of the MDDBR when pumped with pulse energy of 100 pJ.

	$\Delta n, \Delta k(\times 10^{-3})$	
λ_{pump}	Nonthermal	Thermal
500 nm	4, 8	2, −4
720 nm	1, 2	0.5, −1

Put in context of the Kerr effect ($\Delta n = n_2 I$, where I is the optical intensity), when pumping at 500 nm the nonlinear refractive index (n_2) is 1.5×10^{-11}cm^2/W for the nonthermal response and 7.7×10^{-12}cm^2/W for the thermal.

The change of the extinction coefficient (Δk) is found to have opposite sign for the two responses, essentially indicating an increase in the gold absorption for the nonthermal and decrease for the thermal. The increase in absorption of the nonthermal response is a consequence of the interband transitions (usually around 500 nm for gold) effectively turning on at the longer wavelengths of the probe. This is because the nonthermal distribution leads to empty electronic states over a wide range of energies below the Fermi level,[19] hence enabling interband transitions at these energies. However, the decreased absorption for the thermal response is due to a modification to intraband transitions as a consequence of the elevated electron temperature. In the power dependence discussed below in Sec. V B, it is shown that the electron-phonon scattering rate decreases with increasing pump power, and thus increasing electronic temperature. By considering the Drude model, a decrease of the electron scattering rate decreases the damping coefficient and consequently the extinction coefficient.

The magnitude of the response for the same power when pumping at 720 nm is four times smaller than at 500 nm, as expected from the absorbed power. The integrated absorbance of the MDDBR at 500 nm is 80%; whereas at 720 nm, it is 20%; [see Fig. 5(a)]. Therefore the absorption affects the portion of the pump deposited in the sample and as such the magnitude of the change in refractive index. However, we note that at 720 nm, layers 2 and 4 actually absorb more light than at 500 nm. This leads to the predicted and observed differences in the responses when pumping at the two wavelengths, in particular, the change in the sign of ΔR_N at around 600 nm. Hence the response of this system to selective energy injection at specific pump wavelengths does not depend only on the intensity but also on the details of the optical Bloch modes in such devices. Samples with higher numbers of multilayers will have spectrally sharper resonances and hence produce a larger nonlinear response.

The changes in the Bloch modes can be followed by examining the zone-folded miniband dispersion under the conditions of the pump-perturbed dielectric properties of the different metal layers. The changes to the dispersion caused by independently modifying the real and imaginary parts of the refractive index are separately examined and shown in Figs. 4(c) and 4(d). While enhancing the absorption leads to the blue shift of the entire dispersion relation almost rigidly, the real part of the refractive index has a much more complicated

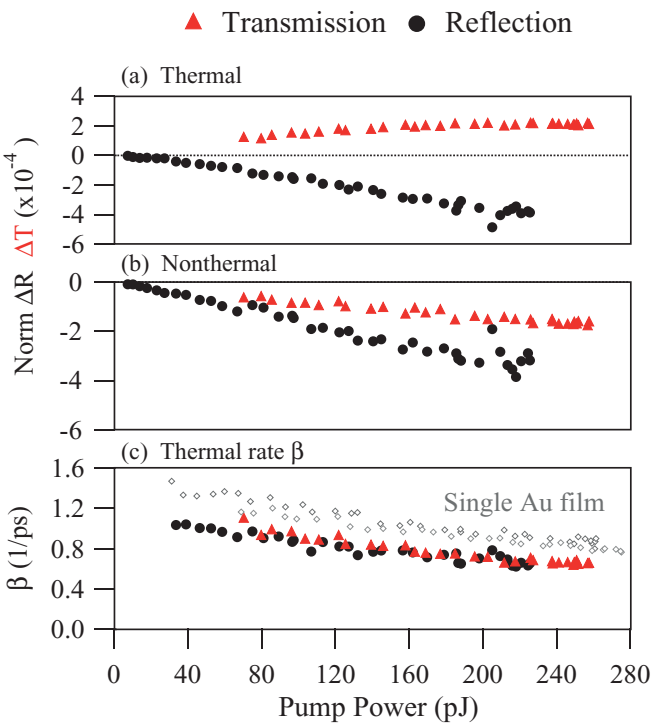

FIG. 7. (Color online) Power dependence of the (a) thermal and (b) nonthermal MDDBR response when pumping at 500 nm and probing at 600 nm. The dependence of β to power in (c) is compared to a single Au film (grey).

effect and significantly distort the dispersion in an asymmetric fashion. These modifications to the dispersion lead to changes in short-pulse propagation through such structures, which is of some interest once the fabrication of large stacks becomes better controlled.

B. Power dependence

The pump power dependence is investigated when pumping in the high-absorption region at 500 nm and probing at the peak of the stopband at 600 nm (Fig. 7). A linear dependence of the amplitude of the response (N, T, and L) is observed in line with results from a single Au layer in the literature.[8] The direction and overall magnitude of the response reflect the spectral variations reported in Sec. V A and is expected to vary with probe wavelength.

In contrast to the single bilayer, a small nonlinearity is observed in the response of the MDDBR, particularly in the thermal component, which is not accounted for by our model. Reproducibility of these results confirms that it is not attributed to sample damage. This can potentially be explained by a variation of the pump electric field profile inside the MDDBR within the duration of the pump pulse. In our model, we do not consider how the change in the dielectric function of the metal layers dynamically alters the pump electric field profile. The metal response is ultrafast and thus varies within the duration of the pump pulse, modifying the propagating pump field profile and thus the deposition of energy at different depths inside the sample. A further cause of this nonlinearity could be the diffusive decay of the nonthermal component, since energy is lost by the diffusion of hot electrons into the surrounding

metal and even the adjacent polymer layers, leading to a lower temperature of the thermal electrons than otherwise predicted.

The electron-phonon scattering rate β is found to decrease linearly with power [see Fig. 7(c)], as expected from the two-temperature model.[16] As the electron temperature increases, the smearing of the Fermi surface increases the number of unoccupied states, thus increasing the electron heat capacity. As the heat capacity of the lattice is larger than the electronic part, the difference in the heat capacities decreases with an increase in electron temperature, thus reducing the thermal exchange rate between the two. However, since each layer in the stack sees a different fraction of the pump energy [see Fig. 5(b)], β will also vary in different layers. The measured value is therefore an average of the contributions of all the layers. This is the cause of the difference in the measured decay constants between the multilayer and a single layer. We find that the electron-electron scattering rate (α) is constant in the results presented here, with a value of 2.75 ps^{-1} obtained by averaging the extracted values of fits at various pump powers and probe wavelengths.

C. Long-lived response

The MDDBR structures are found to have a strong long-time ($>\mu s$) response compared to single Au bilayers. The offset signal (see Fig. 2) is caused by the residual response produced from the previous pump pulse, 4 μs earlier. This response arises from remaining heat that has not diffused away from the excitation spot. The fact that the long-lived response is not observed in the single bilayer suggests the residual response is from the PDMS spacers. Changes in the polymer layer do not cause a significant ΔR or ΔT in a single bilayer, however, they have a significant and measurable effect on the optical resonances on the MDDBR presented here.

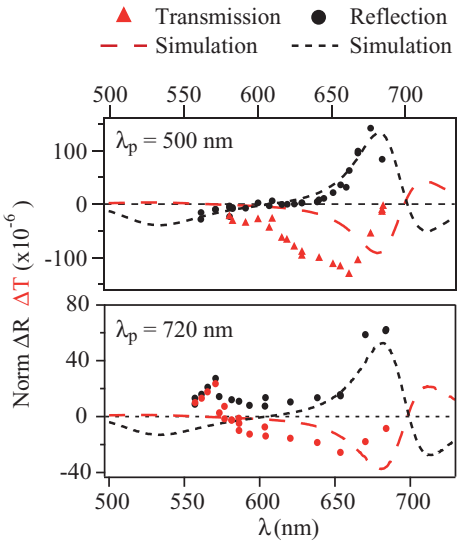

FIG. 8. (Color online) Long-lived response when pumping at 500 and 720 nm at various probe wavelengths. The dashed lines show the expected response for an increase of the polymer layers by a total of 8 pm.

The observed response is best fit in our model by a total increase of the optical thickness of the PDMS layer by 8 pm (see Fig. 8). A fraction of this total thickness change is applied to each layer in proportion to the average optical intensities in the adjacent metal layers. We note that it is the optical thickness that changes (including any temperature dependence of the PDMS refractive index) and it is not strictly a change in the polymer layer thickness.

Good agreement is again found between the modeled and measured reflection response. The measured transmission response, however, is blue shifted with respect to the expected response from the model. Furthermore, there are some strong deviations from the model when pumping at 720 nm, particularly at shorter wavelengths. A complete model for the long-lived response would require the full simulation of the heat diffusion in this complicated structure. Layers at different depths in the structure are expected to have different cooling rates. Even within each polymer layer the heat distributions vary depending on the local pump field distribution and proximity to the gold layers. Nevertheless, the results from our simplified simulation presented here demonstrate the sensitivity of such resonant structures, with the ability to measure a change in the optical thickness equivalent to a few picometers.

VI. CONCLUSION

We have shown how the nonlinear behavior of MDDBR structures is dominated by changes of the optical resonances stemming from the nonlinear dielectric function of nm-scale metal films. The explanation of the complex dynamics of the energy relaxation is shown to require the separation of the nonthermal and thermal responses of the metal layers. Moreover, employing such resonant optical structures gives the ability to selectively excite different depths within the structure with nm-scale precision by appropriately selecting the excitation wavelength. Furthermore, the resonant nature of these optical structures effectively amplifies the nonlinear response, giving the ability to resolve small perturbations of the optical structure. Optically exciting these MDDBRs modifies their Bloch dispersion, producing optical intensity-dependent nonlinear dispersions. The transient nonlinearities were found to be of focusing nature with relatively high n_2 values. These are thus suitable systems to observe nonlinear temporal solitons and other phenomena incorporated in the nonlinear wave equations, such as spatial solitons[24] (known as optical bullet holes). We envisage that such optically resonant structures can be used to tailor the nonlinear response in a subtle manner for these nanostructured metal-dielectric hybrid materials, producing a range of new phenomena and potential devices.

ACKNOWLEDGMENTS

The author wishes to thank James T. Hugall (University of Cambridge) for developing the data processing interface, which enabled the effective analysis of the data presented here. We acknowledge financial support by EPSRC EP/G060649/1 and EP/F059396/1.

[1]R. S. Bennink, Y. K. Yoon, R. W. Boyd, and J. E. Sipe, Opt. Lett. **24**, 1416 (1999).
[2]N. Gibbons, J. J. Baumberg, C. L. Bower, M. Kolle, and U. Steiner, Adv. Mater. **21**, 3933 (2009).
[3]N. N. Lepeshkin, A. Schweinsberg, R. S. Bennink, and R. W. Boyd, Phys. Rev. Lett. **93**, 123902 (2004).
[4]G. Ma and S. H. Tang, Opt. Lett. **32**, 3435 (2007).
[5]G. D'Aguanno, N. Mattiucci, M. J. Bloemer, and M. Scalora, Phys. Rev. E **74**, 036605 (2006).
[6]A. Husakou and J. Herrmann, Phys. Rev. Lett. **99**, 127402 (2007).
[7]T. Lee, A. Bristow, J. Hubner, and H. van Driel, J. Opt. Soc. Am. B **23**, 2142 (2006).
[8]T. Ergin, T. Benkert, H. Giessen, and M. Lippitz, Phys. Rev. B **79**, 245134 (2009).
[9]R. Rosei, F. Antonangeli, and U. M. Grassano, Surf. Sci. **37**, 689 (1973).
[10]D. T. Owens, C. Fuentes-Hernandez, J. M. Hales, J. W. Perry, and B. Kippelen, J. Appl. Phys. **107**, 123114 (2010).
[11]Y. Ping, D. Hanson, I. Koslow, T. Ogitsu, D. Prendergast, E. Schwegler, G. Collins, and A. Ng, Phys. Plasmas **15**, 056303 (2008).
[12]E. Xenogiannopoulou, P. Aloukos, S. Couris, E. Kaminska, A. Piotrowska, and E. Dynowska, Opt. Commun. **275**, 217 (2007).
[13]N. Rotenberg, A. D. Bristow, M. Pfeiffer, M. Betz, and H. M. van Driel, Phys. Rev. B **75**, 155426 (2007).
[14]W. S. Fann, R. Storz, H. W. K. Tom, and J. Bokor, Phys. Rev. Lett. **68**, 2834 (1992).
[15]V. E. Gusev and O. B. Wright, Phys. Rev. B **57**, 2878 (1998).
[16]J. Chen, D. Tzou, and J. Beraun, Int. J. Heat Mass Transf. **49**, 307 (2006).
[17]J. Bigot, Chem. Phys. **251**, 181 (2000).
[18]E. Carpene, Phys. Rev. B **74**, 024301 (2006).
[19]C. K. Sun, F. Vallee, L. H. Acioli, E. P. Ippen, and J. G. Fujimoto, Phys. Rev. B **50**, 15337 (1994).
[20]A. Kavokin, J. J. Baumberg, G. Malpuech, and F. P. Laussy, *Microcavities* (Oxford University Press, Oxford, 2007).
[21]P. B. Johnson and R. W. Christy, Phys. Rev. B **6**, 4370 (1972).
[22]J. M. Bendickson, J. P. Dowling, and M. Scalora, Phys. Rev. E **53**, 4107 (1996).
[23]M. Ghulinyan, C. J. Oton, Z. Gaburro, L. Pavesi, C. Toninelli, and D. S. Wiersma, Phys. Rev. Lett. **94**, 127401 (2005).
[24]W. J. Firth and A. J. Scroggie, Phys. Rev. Lett. **76**, 1623 (1996).